Advanced Microgrid: Containerized Development Platform

João Marcus S. Callegari[1]**, Danilo I. Brandao**[1]**, Luís Guilherme M. Oliveira**[2]**,**
Sidelmo M. Silva[1]**, and Braz J. Cardoso Filho**[1]

[1]Universidade Federal de Minas Gerais, Graduate Program in Electrical Engineering, Belo Horizonte, MG, Brazil.
[2]Pontifícia Universidade Católica de Minas Gerais, Department of Electrical Engineering, Belo Horizonte, MG, Brazil.

e-mail: jmscallegari@ufmg.br; dibrandao@ufmg.br; luis.monteiro@gmail.com; sidelmo@ufmg.br; braz.cardoso@ieee.org

ABSTRACT This paper presents a containerized development platform suitable for developing and validating advanced microgrids (MGs). Through a collaborative effort involving the Federal University of Minas Gerais (UFMG) within the technical-scientific research project titled Minirrede Oasis-UFMG and the State and Federal government, the Tesla containerized MG emerges as a physical simulation tool on advanced MG projects in both islanded and grid-connected operating modes. Installed at the Tesla Laboratory located in the UFMG School of Engineering, Brazil, Tesla MG is composed of (i) eleven distributed energy resources (DERs), which supply around 33 kW; (ii) one single-phase gas-driven synchronous generator (SG), with a power rating of 11 kW; (iii) one 7.5 kW three-phase diesel-driven SG; and (iv) 30 kVA 4-quadrant programmable AC load and source. All these devices are commercially available off-the-shelf equipment. Photovoltaic modules and different battery technologies are installed outside and inside the container, respectively, with cabling extending to the container to connect these components to the inverters. Hardware-in-the-loop (HIL) platforms for real-time simulations (i.e., Opal RT OP5700 and Typhoon HILs 402 and 604) are also available to support MG research. Experimental results are provided to demonstrate the capabilities of the Tesla MG, specifically focusing on inverter features, power dispatchability in grid-connected mode, and proper operation in islanded mode.

KEYWORDS Advanced microgrid, container, distributed energy resource, flexible control.

I. INTRODUCTION

The adverse effects of widespread penetration of non-dispatchable distributed energy resources (DERs) in low-voltage (LV) distribution grids are mitigated with advanced microgrid (MG) models [1]. The term MG commonly refers to systems that ensure a continuous power supply during extreme weather-related outages. Traditional definitions of MGs initially focused on the concept of islanding, which are classified as basic MGs. Essentially, a basic MG is designed solely for resilience, applied to mission-critical facilities. It consists of several loads (both critical and curtailable) and features a control mechanism that disconnects the MG from the utility grid to create an islanded power system. The scenario considered in this paper involves the concept of advanced MGs, which differ from basic MGs [1]. Advanced MGs have emerged later, integrating multiple DER technologies and providing benefits such as energy cost reduction, reduced carbon emissions, participation in grid market transactions, ancillary services support, efficient operation with power dispatch, and reduced line losses. The advanced MG model not only creates an island grid but also enhances the grid hosting capacity. It improves grid power quality, efficiency, and the provision of ancillary services through proper coordination of DERs. Although definitions for these variations of MGs are not yet consolidated in the literature, an advanced MG structure should comply with the following criteria [2], [3]: (i) inherent power sharing among DER units for efficient operation; (ii) regulation of power exchanged with the upstream grid to function as a single controllable entity; and (iii) capability of operating in both grid-connected and islanded modes to ensure high system reliability. The advanced MG model groups loads and DERs into electrically well-defined boundaries, providing a solution for effective power flow control, effective voltage control, support for higher penetration of intermittent renewable energy sources, and improved power quality by offering auxiliary services related to high-capacity coordination. In addition to coordinating DERs effectively, the advanced MG model also minimizes the undesired side effects of their local operation and enhances the use of DER power capabilities.

Committed to sustainable policies and positioned at the forefront of technology, the Federal University of Minas Gerais (UFMG) has approved a technical-scientific research project titled Minirrede Oasis-UFMG [4]. This project aims to enhance electricity self-generation and advance MG technology. By 2024, the project plans to install and integrate three photovoltaic (PV) plants (129 kWp, 229 kWp, and 148 kWp), 200 kW/300 kWh of battery storage, and a 130 kW gas microturbines, coordinating these assets as an advanced MG to power 50 academic buildings with a total installed capacity of 12.2 MW. To date, all 506 kWp of the PV capacity has been installed, while the remaining components

are in the commissioning phase. To support this enterprise, the so-called Tesla containerized advanced MG is installed at Tesla Laboratory - UFMG and emerges as a smaller-scale experimental tool for designing, developing, and testing islanded and grid-connected MGs. This experimental test platform will yield knowledge, valuable insights, and inputs for the deployment of the large-scale Minirrede Oasis-UFMG.

Universities, industries, and research institutions have developed their own MG test facilities. The report compiled in [5] periodically discloses the state-of-the-art of smart grid laboratories. Among the 86 research laboratories, around 60% produce research on MGs, and only two of them are located in Brazil. In addition to the laboratories located at the Federal University of Sao Paulo [6] and at the State University of Campinas [7], both addressed in [5], other MG research laboratories can be found in the following Brazilian institutions: Federal University of Santa Catarina [8], Federal University of Santa Maria [9], Federal University of Maranhão [10], Federal University of Uberlândia [11], Federal University of Itajubá [12], and others. Despite technological advancements, significant national effort is still required in developing experimental MG testbenchs to achieve greater recognition in the international scenario.

Worldwide, the authors of [13] compare MGs from different regions and also look at real-world MG testbeds. Also, reference [14] surveys university MG testbeds from the U.S. and worldwide, classifying them into three types: simulation-based, hardware-in-the-loop (HIL)-based, and physical testbeds. Reference [15] shows a containerized test facility for design validation of MGs, addressing voltage, frequency, and mode transition tests. This MG is equipped with a diesel generator, different renewable energy sources, a battery energy storage system (BESS), protection relays, power-quality meters for each DER, and others. The authors of [16] discuss the deployment, implementation, and commissioning of two distinct energy management systems for a MG testbed situated in Canada. The testbed detailed in [17] is designed for testing and evaluating performance in a real desert environment. It includes PV systems of various technologies, microturbines, diesel generators, energy storage system (ESS), loads, and an industrial MG central controller (CC). Reference [18] shows an optimal MG planning method that integrates a hydrogen energy system in a MG lab facility at Austria.

Reference [19] presents a survey on the availability and implementation of MG test systems in various countries throughout Sub-Saharan Africa. The authors of [20] developed a experimental DC microgrid for rural electrification in Sub-Saharan Africa and Southeast Asia, deployed in Madagascar. It connects small nanogrids to increase electricity access and improve the economic sustainability of the region. Reference [21] proposes a MG testbed for the Middle East and North Africa, which integrates hybrid renewable energy sources and ESSs to effectively supply loads rated at approximately 500 kW. Reference [22] outlines the design features of existing MGs, drawing on insights from the development of a MG laboratory in Italy.

Reference [23] shows a proof-of-concept containerized MG solution designed for disaster response applications. The prototype is thoroughly discussed through each phase of the engineering design process, including design requirements, system sizing and component selection, integration and fabrication, and commissioning and performance testing. Reference [24] shows an integrated MG laboratory system, comprising multiple DERs, a diesel generator for backup, and a flywheel for fast power balancing. Akipolat et al. [25] address the design, modeling, implementation, and operation of a standalone hybrid power MG for an education and research laboratory. Reference [26] proposes an economic and environmental assessment of a flexible pilot facility for testing various smart microgrid configurations as a living test-bed laboratory. Reference [27] shows a MG laboratory that supports various simulations and provides hands-on experience for students. The paper [28] introduces a comprehensive AC/DC laboratory setup that integrates a PV system, BESS, and a small hydropower plant, with a SCADA system to ensure coordinated operation and demonstrate its wide-ranging potential through experimental results. The authors of [29] present a comprehensive MG testbed, which includes various primary resources, a smart switchboard, and loads integrated into a SCADA system for real-time monitoring and control.

Although research has been done so far on this topic, practical integration into distribution grids is still at an early stage, especially in Brazil. Thus, this paper shows some challenges, practical aspects, and experimental results to reduce the gap between MG prototypes and practical MG. This paper is an extended version of [30], providing an enhanced state-of-the-art description, presenting additional experimental results, and detailing further constructive aspects of the Tesla containerized MG. Since container-mounted systems are flexible and compact mobile platforms with a small footprint, this structure is chosen for the development of the Tesla advanced MG. These containerized systems reduce engineering and installation costs, offering plug-and-play and portable features. This configuration provides significant advantages in terms of rapid deployment, cost-effectiveness, and adaptability for various applications, including remote communities and disaster response scenarios. In such an approach, Tesla MG employs the well-established hierarchical three-level centralized control architecture, in which the DERs are coordinated by means of the power-based control (PBC) algorithm [31]. Other secondary-level control formulations can be employed without loss of generality. This paper shares all constructed infrastructure and design considerations with the research community, highlighting the flexibility of the experimental tool as many parts can be reconfigured.
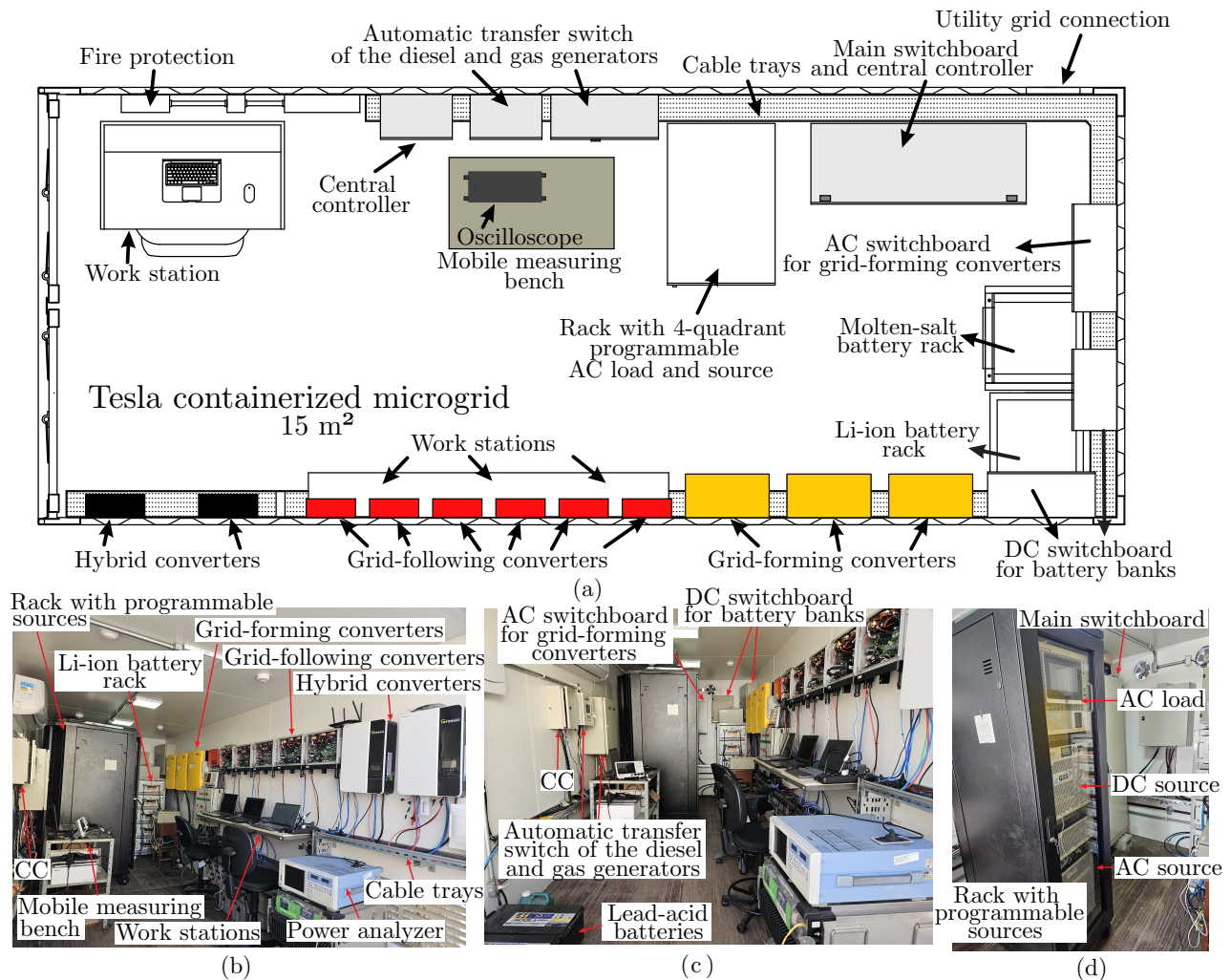
FIGURE 1. **(a) Layout design of the Tesla containerized MG facilities. (b)-(d) MG physical facilities.**

This paper is outlined as follows: Section II presents the Tesla containerized MG facilities. Section III shows the MG control organization. Section IV shows experimental results regarding MG operating in grid-connected or islanded modes. Conclusions are stated in Section V.

II. TESLA CONTAINERIZED MICROGRID

The physical facilities of the Tesla containerized MG are shown in Figure 1, installed at the Tesla Power Engineering Laboratory at UFMG School of Engineering (SE-UFMG), Brazil. The standard 20-ft maritime container comprises approximately 15 m^2 with some workstations (WSs) organized as shown in Figure 1(a). The minimum thickness of the carbon steel lining the container is 2 mm. The walls and ceiling are filled with high-density EPS panels between carbon steel materials for thermal insulation purposes. The container has hooks that allow MG mobility as a plug-and-play solution. The floor is moisture-resistant, has anti-mold and anti-insect treatment, does not warp, and does not spread fire. Figure 1(a) shows the layout design of the equipment

inside the MG container, while Figures 1(b), (c), and (d) show the internal physical installations. The MG is supplied by 220 V and 440 V AC circuits from the UFMG grid, as shown in Figure 2(a). Both circuits are derived from 500 kVA~13.8-0.22 kV (60 Hz) and 500 kVA~13.8-0.44 kV delta-star transformers installed at SE-UFMG substation. Gauge cables of 70 mm^2 and 25 mm^2 are derived from the UFMG electrical power system to the MG main switchboard. Upstream 150 A/ 45 kA and 70 A/ 20 kA circuit breakers ensure thermomagnetic protection of the Tesla containerized MG.

All internal MG circuits are derived from the main switchboard, where voltage and current measurements are acquired by the MG CC. The Texas Instruments LAUNCHXL-F28379D digital signal processor (DSP) is adopted to process the CC algorithm. The upstream grid can be formed by the utility grid (i.e., circuit 1, fed by the UFMG internal grid, as shown in Figure 2(a)) or by a programmable 30 kVA 4-quadrant AC source - see circuit 2 in Figure 2(b). The 4-quadrant programmable source is installed inside the
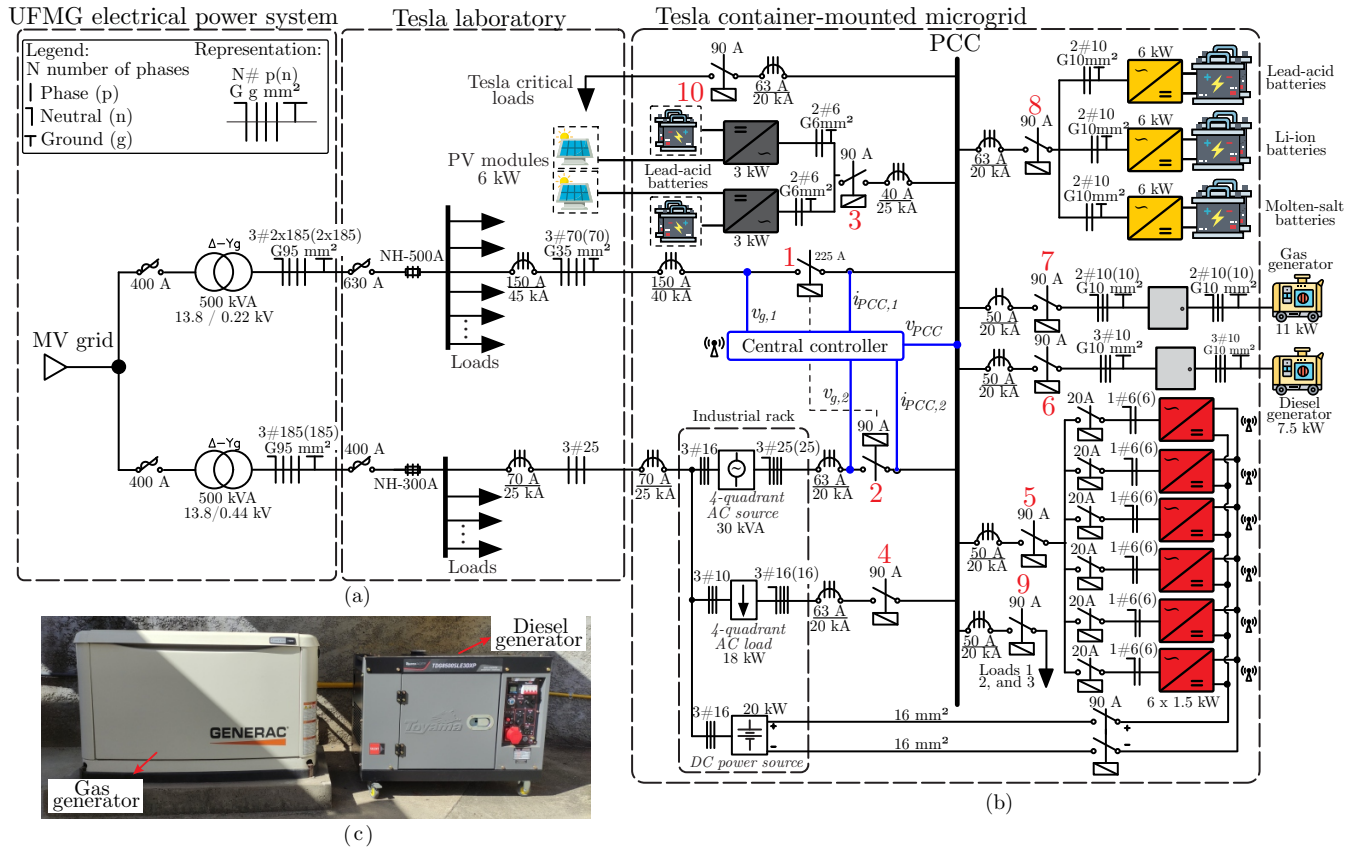
FIGURE 2. (a) UFMG electrical power system that supplies the Tesla containerized MG. **(b)** Electrical schematic of the Tesla containerized MG facilities and structures. **(c)** Synchronous generators driven by gas and diesel engines, both installed outside the container.

MG container, and arranged into a 19" industrial rack. An interlocking logic is implemented for both power sources not to simultaneously supply the main MG switchboard. Three-phase current measurements $i_{pcc,1}$ (i.e., utility grid) and $i_{pcc,2}$ (i.e., programmable AC source) are acquired and instrumented on the CC analog-to-digital (ADC) channels. Three-phase voltages upstream of contactors 1 and 2 (i.e., $v_{g,1}$ and $v_{g,2}$), and at the MG PCC (i.e., v_{pcc}) are also measured by the CC.

Four-quadrant programmable load, with 18 kW power rating, is arranged inside the 19" industrial rack, and operated through circuit 4 in Figure 2(b). The programmable load allows the emulation of constant active and reactive (PQ) power loads, constant impedance-type (Z) loads, and distorted non-linear loads. HIL platforms for real-time simulations (i.e., Opal RT OP5700 and Typhoon HILs 402 and 604) are also available. These devices allow verifying technical challenges in a controlled simulation environment, before performing experimental tests.

The main switchboard is responsible for load shedding, generation, transitioning between grid-connected and islanded modes, and all relevant tests required by the Minirrede Oasis-UFMG. As noted in Figures 1(a) and 2(b), the MG is deployed using off-the-shelf commercial grid-following, grid-forming, and hybrid DERs. For instance, the

three off-the-shelf single-phase grid-forming Sunny Island 6.0H inverters (from SMA) are shown in Figures 1(a), which are DC-supplied by lead-acid, li-ion, and molten-salt batteries. The batteries 12MS234 (48V and 220 Ah capacity), FZ SoNick SA 48TL200 (48 V, and 200 Ah capacity), and Unicoba UPLFP48-100 (48 V and 100 Ah capacity) are installed at the back of the container, as shown in Figure 1. Contactor 8 is responsible for galvanically connecting the SMA inverters to the MG switchboard, as shown in Figure 2(b). The SMA inverters are delta-connected forming a three-phase grid in a master-slave configuration, capable of providing services in grid-connected and islanded modes by charging or discharging the battery bank. Figure 1(a) shows the installation layout of two 3 kVA Growatt hybrid off-grid inverters, while Figure 2(b) shows the electrical circuit 3 connecting the Growatt inverters to the MG switchboard. These hybrid inverters are powered by 6 kW PV strings installed on the rooftop of SE-UFMG and DC-supplied by lead-acid batteries.

Depending on their role in AC MGs, power converters can be classified into grid-feeding, grid-supporting, and grid-forming converters. Grid-feeding power converters are primarily designed to deliver power to the grid, acting as controllable current sources perfectly synchronized with their point of connection (PoC) voltage. Despite being able to

TABLE 1. Main off-the-shelf equipment of the Tesla containerized advanced MG.

Description	Quantity	Part number
Grid-connected inverters	6	PHB 1500-NS
Hybrid off-grid inverters	2	SPF 3000TL LVM-ES
Hybrid grid-connected inverters	3	Sunny Island 6.0H
PV modules	24	Yingli 245P-32
Li-ion batteries	5	Unicoba UPLFP48-100
Molten-salt batteries	2	FZ SoNick SA 48TL200
Lead-acid batteries	4	12MS234
Diesel generator	1	TDG8500SLE3DXP
Gas generator	1	Generac Guardian 11
4-channel oscilloscopes	1	MSO7034B
	1	MSO7014
	1	DHO804
Power analyzer	1	Yokogawa WT1800
4-quadrant AC load	1	NHR 9430
4-quadrant AC grid	1	TC.ACS.30.528.4WR.S.LC
Bidirectional DC power supply	1	TC.GSS.20.500.400.S.HMI

operate in grid-connected, grid-forming power converters are also responsible for establishing a stable voltage and frequency in an islanded MG. This is the case with the SMA and Growatt inverters installed at Tesla MG.

There are six programmable grid-following PHB 1500-NS inverters, which consist of a current-controlled DC-AC full-bridge converter with a passive LC output filter. The factory firmware is deleted and flexible control strategies for all desired applications are programmed. As shown in Figure 2(b), contactor 3 is used to connect the inverter to the MG switchboard. The factory firmware is deleted and flexible control strategies for all desired applications are programmed. The control strategy implemented at the PHB inverters is in accordance with [32], [33]. PHB inverters are equipped with communication units, and the necessary apparatus for their connection to the MG. The DC-side is supplied by the rectified voltage from a DC power source, as shown in Figure 2(b). The DSP embedded in PHB 1500-NS inverters is programmed and debugged via an XDS110 JTAG controller.

The automatic transfer switch (ATS) of two synchronous generators (SGs) are arranged as shown in Figure 1(a) and are responsible for the automatic and safe transfer from one power source to another during grid outages. The automatic voltage (i.e., AVR) and frequency (i.e., governor) controls are embedded in the SGs. The electrical control panels of SGs are represented by circuits 6 and 7 in Figure 2(b). The SGs are driven by gas and diesel engines, respectively. Figure 2(c) shows the single-phase 11 kW gas-driven and three-phase 7.5 kW diesel-driven SGs, installed outside the container. Both SGs have black-start capability to act as the grid-forming units. For instance, the diesel-driven SG supplies Tesla laboratory critical loads in case of grid outages. The SGs can be operated in isochronous mode, droop mode,

and PQ mode with remote-control capability. In summary, Table 1 lists the main off-the-shelf equipment of the Tesla containerized advanced MG, along with the respective part numbers. The electrical switchboards shown in Figure 2 are all custom-built for the Tesla MG.

III. TESLA MICROGRID CONTROL ORGANIZATION
The control of the Tesla MG is developed in three hierarchical levels according to Figure 3. The primary level is responsible for the embedded operation of the DERs and SGs. This control level is decentralized, and each DER unit has its own primary control. For instance, voltage and frequency control in SGs, along with power sharing, are overseen by the primary level.

The primary and secondary levels of the MG hierarchical control communicate with each other through a low-bandwidth control area network (CAN) infrastructure. The CAN network runs inside the container in a dedicated conduit and uses two shielded/twisted pair wires as the physical transmission link, with a transmission rate of 125 kbps. All off-the-shelf equipment with CAN support are connected to this internal network. Local operational data from the primary level is transmitted to the CC at each control cycle, as shown in Figure 3.

The secondary level is represented by CC, where well-established PBC is implemented [31]. This strategy coordinates DERs by a central unit (i.e., CC) located at the PCC, providing controlled active and reactive power flow to the upstream grid. The features of this control level are: proportional power sharing among DERs; power flow control at the MG PCC in grid-connected mode; and management of the grid-connected and islanded modes. From the latter, the SGs and/or SMA DERs are responsible for imposing voltage and frequency in islanded mode. Also, PBC requires low implementation complexity, and minimum requirements in terms of communication infrastructure (i.e., narrowband and low data rate communication). It supports plug-and-play integration of new DERs and does not require previous knowledge of the MG parameters. The data exchanged be-
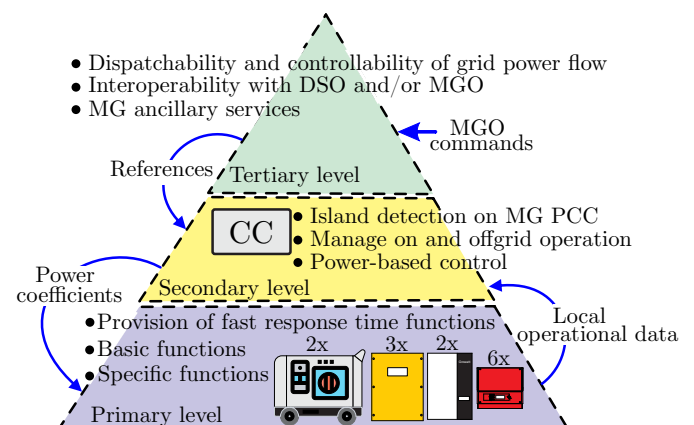
FIGURE 3. Tesla MG hierarchical control architecture.

tween the CC and DERs consists only of average values (i.e., time-varying values with slow dynamics). Once the CC gathers all necessary information from the DERs (i.e., primary level — see Figure 3), it transmits power coefficients [31] to the primary level to adjust the power output of the DERs within operating limits to meet one of the following control objectives at the MG PCC: (*i*) achieve self-consumption condition; (*ii*) import or export active and reactive power; and (*iii*) other services not addressed in this work, such as power factor control, upstream grid voltage support, etc. Thus, the CC transmits power coefficients [31] to the primary level. Since the communication is limited to MG support functions, all the functions that are performed autonomously (i.e., primary level) runs normally if communication failures occur.

The tertiary control level performs the interoperability between the MG and external agents, carried out through a Raspberry Pi via the MQTT or UTP protocols. Power dispatch management and slow-dynamics ancillary services are handled at the tertiary control level. At this level, power references are transmitted to the secondary control level. There is no control loop at this level, in which power references are commanded based on the technical or economic interests of the microgrid operator (MGO). Also, references generated by the tertiary level may be in accordance with a mutually agreed contract with the distribution system operator.

IV. EXPERIMENTAL RESULTS

The main parameters of the Tesla MG are shown in Table 2. The ratings of circuit breakers and contactors are shown in Figures 2(a) and (b). The conducted experiments encompassed the following conditions: (*i*) flexible converter control for Tesla MG; (*i*) grid-connected MG operation, showcasing the power dispatchability feature by steering the PHB DERs; and (*ii*) transitions between MG islanded and grid-connected modes. The gas generator operates as a grid-forming unit in this MG islanding scenario. A microSD card-based datalogger is developed in the CC, whose data is acquired every 5 s. The results are acquired by the developed datalogger, along with a 4-channel oscilloscope equipped with A612 and P5200A probes. The communication link between PHB DERs and CC is configured to occur every 1/10 s. The MG loads are adjusted to drain constant active and reactive power, according to Table 2. MG loads are also defined in Table 2. The main parameters of the different nature ESS are also shown in Table 2, where n, V_b, and C_r represent the number of batteries installed in the container, the rated voltage, and the Ah capacity.

A. Flexible converter control for Tesla MG

The Growatt inverters are connected through circuit 3 of the MG switchboard in Figure 2(b), capable of operating as both grid-feeding and grid-forming converters. The latter occurs when supplying power the output critical port in

TABLE 2. Parameters of the Tesla containerized advanced MG.

MG overall parameters	Label	Value
RMS phase-to-neutral voltage	V_g^{RMS}	220 V, 60 Hz
Fundamental line frequency	ω_n	377 rad/s
Loads	L1	75 Ω
	L2	24+j150 Ω
	L3	42 Ω
PHB inverter parameters	**Label**	**Value**
DER power rating	S_n^{PHB}	1.5 kW
Switching/sampling frequency	f_{sw}, f_s	15 kHz
LC filter parameters	L_f, R_f, C_f	2 mH, 150 mΩ, 3.3 μF
DC-link capacitance	C_{DC}	1.17 mF
DC-link voltage	V_{DC}	400 V
PoC peak voltage	V_{pk}	$220\sqrt{2}$ V
PHB inverter controllers	**Label**	**Value**
Inner loop: proportional gain	K_{pi}	16 Ω
Inner loop: integral gain	K_{ii}	1000 Ω/s
Inner loop: crossover freq.	f_{ci}	1000 Hz
Inner loop: phase margin	PM_i	60 deg.
Outer loop: proportional gain	K_{pp}	0.0079 V^{-1}
Outer loop: integral gain	K_{ip}	1.29 V^{-1}/s
Outer loop: crossover freq.	f_{cp}	15 Hz
Outer loop: phase margin	PM_p	75 deg.
Other DER parameters	**Label**	**Value**
SMA DER power rating	S_n^{SMA}	6 kW
Growatt DER power rating	S_n^{GWT}	3 kW
Gas SG power rating	S_n^{Gas}	11 kW
Diesel SG power rating	S_n^D	7.5 kW
ESS parameters	**Label**	**Value**
Lead-acid batteries (12MS234)	n, V_b, C_r	4, 12 V, 220 Ah
Li-ion batteries (Unicoba UPLFP48-100)	n, V_b, C_r	5, 48 V, 100 Ah
Molten-salt batteries (FZ SoNick SA 48TL200)	n, V_b, C_r	2, 48 V, 200 Ah
Central controller parameters	**Label**	**Value**
CC sampling frequency	f_s^{CC}	6 kHz
CC processing frequency	f_{com}	10 Hz

the grid absence. Figure 4(a) shows the equipment block diagram, which comprises: (*i*) unidirectional and bidirectional DC converters that interface the PV modules and batteries, respectively, with the inverter DC-link; and (*ii*) a bidirectional inverter that can operate in grid-feeding or grid-forming mode to meet the demand of the load connected to the equipment's critical output port. Each equipment is powered by a 3 kW rooftop PV string consisting of twelve YL245P PV modules and is DC-supplied by four series-connected 12MS234 lead-acid batteries, providing a total of 48 V and 220 Ah. Contactors within the equipment are responsible for managing the primary source that feeds the inverter's critical port, as shown in Figure 4(a). The priority to supply the critical port by primary energy sources (i.e., PV, grid, or batteries) depends on the operating mode configured in the inverter, which can be: utility grid first (UF), solar first (SF), solar-utility-battery (SUB), or solar-battery-utility

6

Eletrônica de Potência, Rio de Janeiro, v. 30, e202502, 2025.
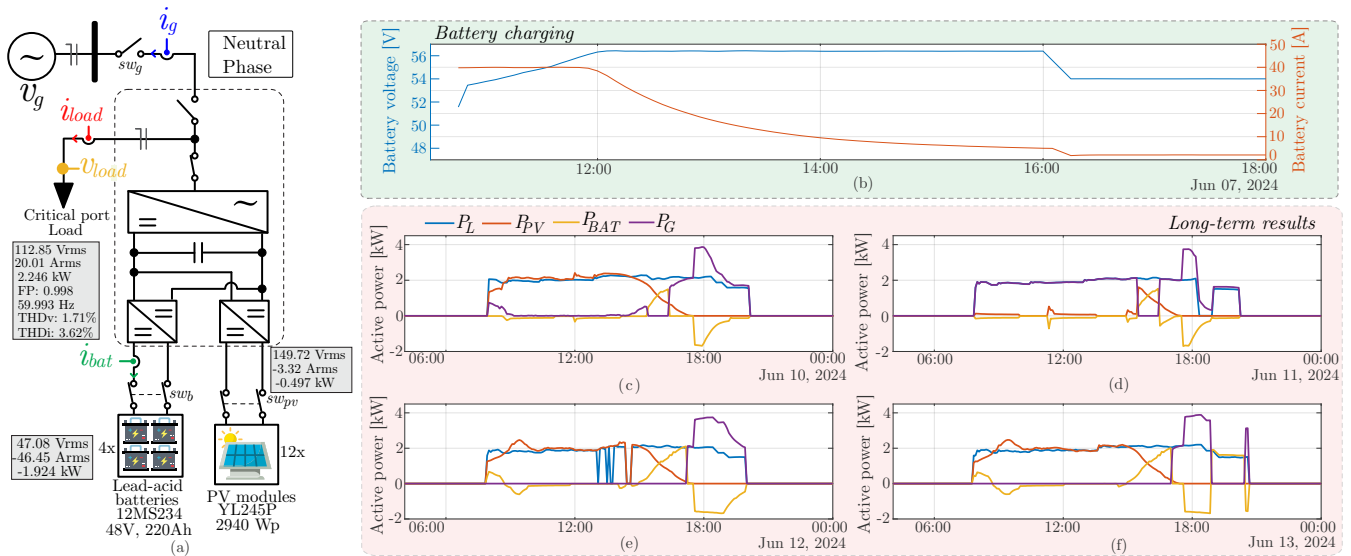
FIGURE 4. Experimental setup composed by the Growatt inverter: (a) schematic block diagram with experimental power measurements at the input and output of the converter, (b) experimental results of lead-acid battery charging, (c)-(f) experimental long-term results for each inverter operating mode.
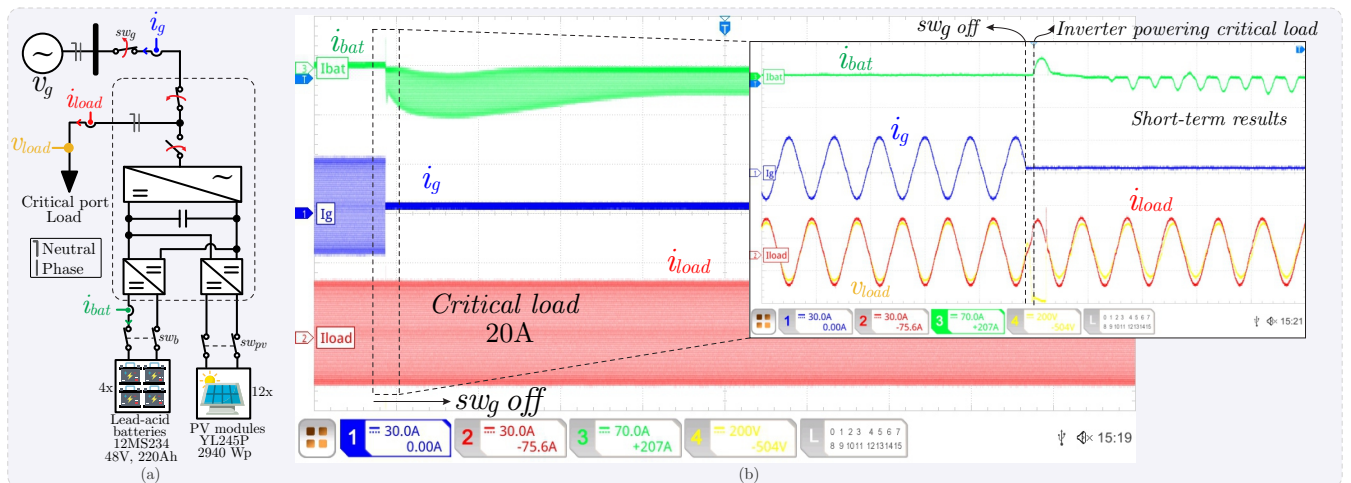
FIGURE 5. Experimental setup composed by the Growatt inverter: (a)-(b) experimental short-term results.

(SBU). The results of Figures 4 and 5 are obtained from this equipment, considering the charge curve of lead-acid batteries, long-term performance for each inverter operating mode, power measurements at the input and output of the converter (e.g., assessment of efficiency or power quality metrics), and short-term performance. Some sampled results are shown in Figures 4(b)-(f), demonstrating the flexibility of this equipment within the Tesla MG context for both didactic and research purposes.

Figure 4(a) displays several power quality parameters of the Growatt inverter in grid-forming mode, supplying power to the critical port. sw_{pv} and sw_b are closed, while sw_g is open. The Yokogawa WT1800 precision power analyzer is used to measure frequency, THDv, THDi, power factor, active power, and other metrics for the critical load, batteries, and PV modules. To supply 2.246 kW to the critical load, 1.924 kW is provided by the batteries and 0.497 kW by the

PV modules, resulting in a conversion loss of 0.175 kW. In grid-forming mode, the voltage and frequency imposed by the inverter on the critical port are 112.85 V and 59.99 Hz, respectively. The quality of the voltage and current is reflected in a low THDv of 1.71% and low THDi of 3.63%. With this experimental setup, the inverter efficiency can be easily raised, along with other relevant analyses.

Figure 4(b) shows the lead-acid battery charge curve as managed by the Growatt inverter. The charging process consists of three stages: The first stage is the constant current mode, where a constant current of 40 A is supplied until the battery voltage reaches the charge boost voltage of 57 V. The second stage is the constant voltage mode, where the voltage remains at 57 V and the current decreases. Once the current drops to approximately 10% of the initial discharge current, the float voltage of 54 V is applied and maintained until a new discharge command is issued. Since the current and

voltage characteristics of the 12MS234 lead-acid batteries are specified by the manufacturer, this parametrization is straightforwardly used during the inverter commissioning.

Long-term results, collected over 24 hours on June 10th and 13th, are shown in Figures 4(c), (d), (e), and (f) for SUB, UF, SF, and SBU modes, respectively. During this period, a programmable load is connected to the inverter's critical port, simulating a typical UFMG building load pu profile with high demand during class hours (i.e., 7 AM to 8 PM). In all cases, sw_g is opened between 3 PM and 4 PM. The power sign convention in Figure 4(c) differs from the one in Figure 4(a) for convenience. Positive power means the primary energy source supplies power, while negative power means it absorbs power. In the SUB operation shown in Figure 4(c), the power supplied to the critical load P_L primarily comes from the PV modules (i.e., P_{PV}). If there is a generation excess, the batteries are charged (i.e., $P_{BAT} < 0$). If the PV power is insufficient, the grid supplements the load power demand. The battery only supplies power to the critical load when PV power is insufficient and the grid is unavailable, as clearly shown when the sw_g is opened between 3 PM and 4 PM. At the end of the afternoon, after reducing the power generated by the PV modules, the grid charges the batteries and provides all the power for the critical load. Figure 4(d) shows the UF operating mode. The grid provides power to the critical load, while the PV system only charges the batteries. When the grid is unavailable(i.e., sw_g opened between 3 and 4 PM), both PV and battery systems supply power to the critical load. In the absence of PV power, the power grid charges the batteries in the late afternoon and at night. In the SF operation shown in Figure 4(e), PV modules supply power to the load with priority. If the PV power is insufficient, batteries provide the additional required power to the critical load. The grid supplies the critical load only if the PV power is unavailable or the battery voltage is low. With the absence of sufficient solar irradiance from the end of the afternoon, the power grid assumes the critical load and also charges the batteries. At last, Figure 4(f) shows the SBU operation. The PV system supplies power to the load with priority. If PV power is insufficient, the battery supplements the required load power. The grid provides power to the load only when the battery is discharged (i.e., at low terminal voltage), which occurs around 5 PM.

Finally, short-term experimental results are shown in Figure 5(a). The circuit breakers sw_g, sw_{pv}, and sw_b are initially closed. In the UF mode, the inverter internally bypasses the grid to connect directly to the critical output port. Subsequently, the sw_g circuit breaker is opened, as shown in the schematic of Figure 5(a). To maintain supply to the critical port in the absence of the grid, the equipment galvanically disconnects from the grid and starts the inverter in grid-forming mode to supply the load. This mode transition occurs in less than one line-frequency cycle, as noted in Figure 5(b). The inverter establishes voltage and frequency to the critical port, initially using the battery bank as the primary source to supply power to the critical load. It is observed that the battery current decreases after a few cycles, indicating that the MPPT has adjusted and the PV system is also contributing to the power supply for the critical port.

B. Controlled PCC power flow in grid-connected mode

In the following results, circuits 1 and 5 are enabled in Figure 2(b), configuring a grid-connected MG operation. PHB inverters communicate via the CAN network with the CC to achieve PCC power flow control. It is noteworthy that the Tesla MG also enables straightforward integration of alternative control formulations at the secondary level. Experimental results are shown in Figure 6 as proof of concept of controlled PCC power flow. Power references for PCC power injection, absorption, and self-consumption operations are provided by the tertiary level through commands from the Raspberry Pi.

Two PHB 1500-NS inverters connected to the same phase are coordinated by the CC (i.e., secondary level), by means of the PBC algorithm. The experimental power terms collected at the MG PCC and at the inverters 1 and 2 terminals are shown in Figure 6(a)-(c), respectively. During the event (i), the inverters operate in stand-by mode with null power injection since the MG control is disabled. The MG control is enabled with self-consumption mode in (ii), in which inverters share power to regulate null PCC active and reactive power terms. In scenario (iii), the desired reactive power reference Q^* is changed from 0 to 500 var to absorb reactive power from the grid, as depicted in the zoomed view of Figure 6(d). Subsequently, Q^* is varied from 500 to 0 var to once again achieve self-consumption in (iv). These same events are repeated in (v) and (vi), adjusting the communication delay between DERs and CC and still achieving MG stable operation. As noted in Figures 6(b) and (c), inverters 1 and 2 proportionally share active and reactive power terms to achieve PCC power controllability.

C. Transition between grid-connected and islanded modes

During this experimental test, circuit breakers 1 and 2 are open, while circuits 3, 7, and 9 remain closed. Figures 7(a)-(d) show a transition scenario from grid-connected to islanded mode during a utility grid outage, which occurs with a short-term voltage interruption (i.e., about 6 s). The detection of the upstream grid islanded condition is performed by a phase failure relay, followed by the prompt start-up of the gas SG within a few seconds. The zoomed views of Figures 7(b) and (c) show grid and SG voltage and current waveforms during the transition, while Figure 7(d) shows the frequency and RMS voltage at the SG output terminals. Despite the transient dynamics (i.e., frequency within 55.88 and 61.71 Hz and RMS voltage dip of 177 V), the steady-state condition is quickly established, ensuring the power supply continuity and safe Tesla MG island operation.
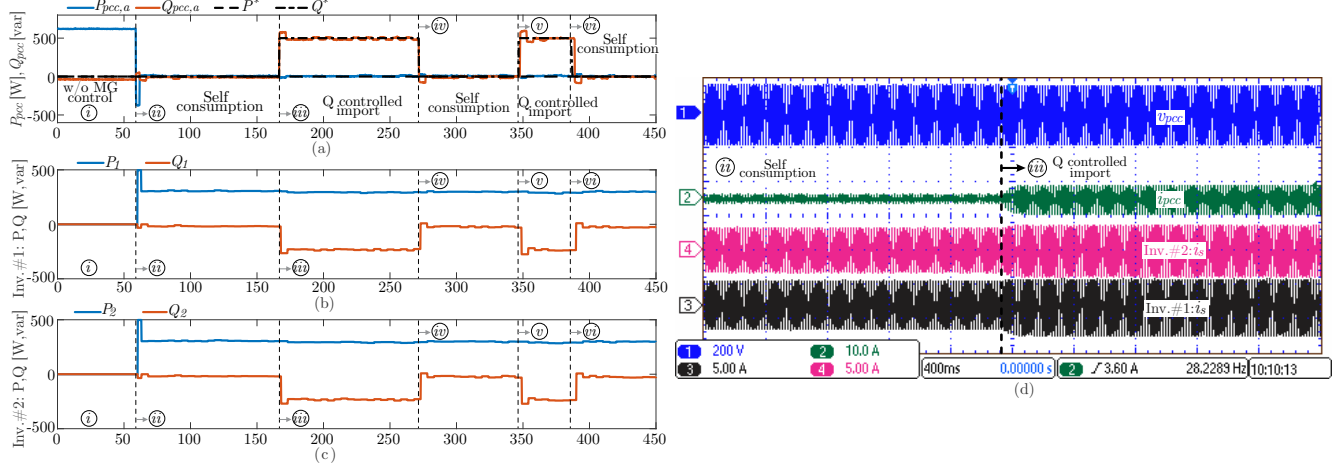
FIGURE 6. (a) Active and reactive power flow at the MG PCC. Active and reactive power terms processed by inverters (b) 1 and (c) 2. (d) PCC voltage and inverter 1 and 2 currents before and after Q^* change from 0 to 500 var.
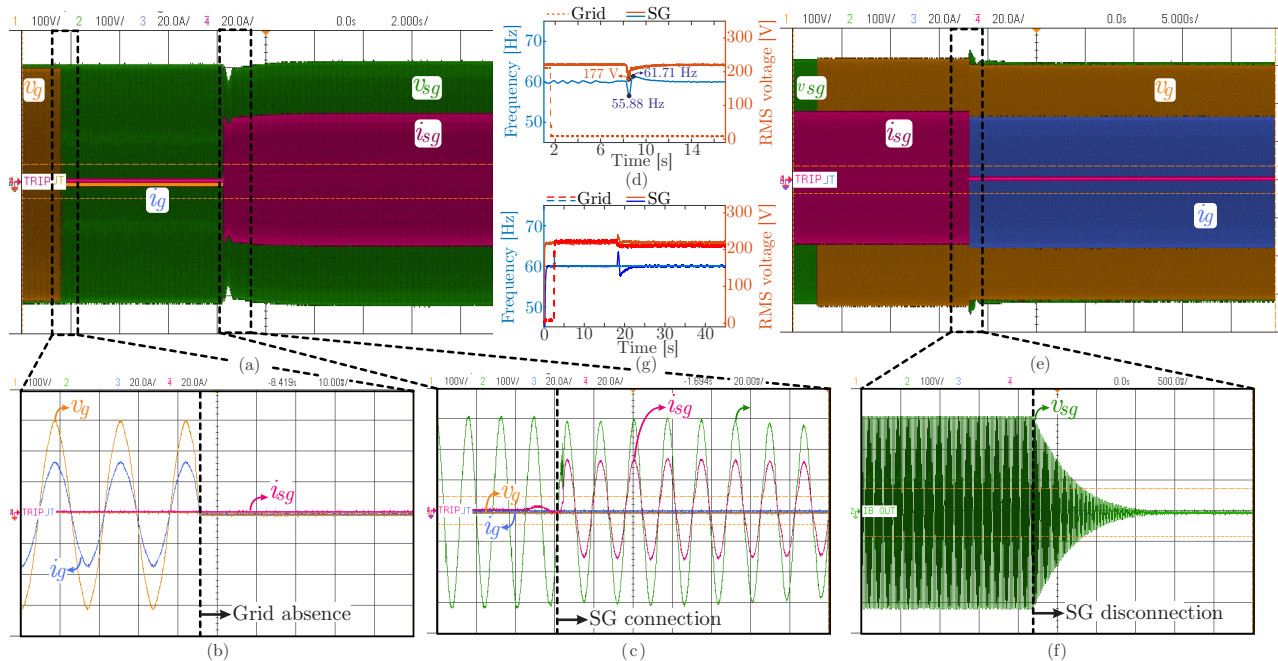
FIGURE 7. Transition from grid-connected to islanded mode: (a) Voltage and current waveforms of the grid and SG. Zoomed views during (b) grid absence and (c) SG connection supplying Tesla MG loads. (d) Frequency and RMS voltage at the grid and SG output terminals. Transition from islanded to grid-connected mode: (e) Voltage and current waveforms. (f) Zoomed view showing the smooth transition between modes. (g) Frequency and RMS voltage at the grid and SG output terminals.

Figures 7(e)-(g) show the islanded to grid-connected transition after the restoration of the utility grid, which occurs smoothly as shown in the zoomed view of Figure 7(f). Once the grid presence is detected, the SG remains to supply Tesla MG loads for approximately 10 seconds before disconnecting and restoring the MG grid-connected mode. Voltage and frequency dynamics during this process do not exceed 10%, as noted in Figure 7(g).

V. CONCLUSIONS

This paper introduced the Tesla containerized MG facilities, highlighting practical implementation aspects of an advanced MG built with off-the-shelf commercial devices. Tesla MG combines suitable hardware, communication infrastructure, and a well-designed three-layer hierarchical control system, providing a flexible platform for conducting MG-related studies. Tesla MG incorporated grid-following and grid-forming DERs with different power ratings, synchronous generators driven by gas and diesel engines, different types of energy storage systems (i.e., li-ion, molten-salt and lead-acid batteries), photovoltaic modules, grid emulator, hardware-in-the-loop simulators, and others. The experimental results demonstrated the effectiveness of the MG control system in achieving power flow controllability, power

Eletrônica de Potência, Rio de Janeiro, v. 30, e202502, 2025.

9

sharing, and proper transition between grid-connected and islanded modes. With an educational focus, experimental results showed a flexible converter operating in both grid-feeding and grid-forming modes, the lead-acid battery charging procedure, long-term operation, and an easy-to-use setup to evaluate converter power quality metrics. These tests showed that Tesla containerized MG is a powerful experimental tool for the deployment of renewable energy sources in advanced MGs, fulfilling many demands of the Minirrede Oasis-UFMG project.

ACKNOWLEDGMENT

AUTHOR'S CONTRIBUTIONS

J. M. S. CALLEGARI: Conceptualization, Data Curation, Formal Analysis, Investigation, Methodology, Software, Validation, Visualization, Writing – Original Draft, Writing – Review & Editing. **D. I. BRANDAO:** Conceptualization, Funding Acquisition, Methodology, Resources, Supervision, Validation, Visualization, Writing – Review & Editing. **L. G. M. OLIVEIRA:** Conceptualization, Methodology, Supervision, Validation, Visualization, Writing – Review & Editing. **S. M. SILVA:** Conceptualization, Funding Acquisition, Methodology, Project Administration, Resources, Supervision, Validation, Visualization, Writing – Review & Editing. **B. J. CARDOSO FILHO:** Conceptualization, Funding Acquisition, Methodology, Project Administration, Resources, Supervision, Validation, Visualization, Writing – Review & Editing.

PLAGIARISM POLICY

This article was submitted to the similarity system provided by Crossref and powered by iThenticate – Similarity Check.

REFERENCES

[1] D. Ton, J. Reilly, "Microgrid Controller Initiatives: An Overview of R&D by the U.S. Department of Energy", *IEEE Power Energy Mag*, vol. 15, no. 4, pp. 24–31, 2017, doi:10.1109/MPE.2017.2691238.

[2] D. I. Brandao, L. S. Araujo, A. M. S. Alonso, G. L. dos Reis, E. V. Liberado, F. P. Marafão, "Coordinated Control of Distributed Three- and Single-Phase Inverters Connected to Three-Phase Three-Wire Microgrids", *IEEE J Emerg Sel Topics Power Electron*, vol. 8, no. 4, pp. 3861–3877, 2020, doi:10.1109/JESTPE.2019.2931122.

[3] IEEE, "IEEE Standard for the Specification of Microgrid Controllers", *IEEE Std 20307-2017*, pp. 1–43, 2018, doi:10.1109/IEEESTD.2018.8340204.

[4] UFMG, "Oásis - UFMG Sustentável", *in online address*, 2023, URL: https://www.ufmg.br/sustentabilidade/projetos/oasis/.

[5] N. Andreadou, I. Papaioannou, A. Marinopoulos, M. Barboni, "Smart Grid Laboratories Inventory 2022", *Publications Office of the European Union*, 2022, doi:10.2760/392963.

[6] L. H. L. Rosa, N. Kagan, C. F. M. Almeida, J. Labronici, S. X. Duarte, R. F. Morais, M. R. Gouvea, D. Mollica, A. Dominice, L. Zamboni, G. H. Batista, J. P. Silva, L. A. Costa, M. A. P. Fredes, "A Laboratory infrastructure to support utilities in attaining power quality and Smart Grid goals", *in ICHQP*, pp. 312–317, 2016, doi:10.1109/ICHQP.2016.7783348.

[7] J. I. Y. Ota, J. A. Pomilio, "LabREI: Ambiente experimental para pesquisas interdisciplinares e formação de recursos humanos em redes inteligentes de energia elétrica", *SBSE*, vol. 1, no. 1, 2021, doi:10.48011/sbse.v1i1.2384.

[8] M. S. Ortmann, V. Maryama, L. J. Camurça, L. C. Gili, D. L. Suarez-Solano, D. Dantas, G. Finamor, V. L. da Silva, L. Munaretto, A. Ruseler, A. G. Andreta, R. F. Coelho, M. L. Heldwein, "Architecture, components and operation of an experimental hybrid ac/dc smart microgrid", *in PEDG*, pp. 1–8, 2017, doi:10.1109/PEDG.2017.7972564.

[9] UFSM, "Instituto de Redes Inteligentes - INRI", *in online address*, 2023, URL: inriufsm.com.br/.

[10] UFMA, "Lab. Microrredes", *in online address*, 2023, URL: portalpadrao.ufma.br/iee/labs/lab-microrredes.

[11] UFU, "Laboratório de Redes Inteligentes - LRI", *in online address*, 2023, URL: lri.ufu.br/unidades/laboratorio-de-redes-inteligentes.

[12] B. P. B. Guimaraes, R. F. Ribeiro Junior, M. V. Andrade, I. A. dos Santos Areias, J. G. L. Foster, E. L. Bonaldi, F. d. O. Assuncao, L. E. d. L. de Oliveira, F. M. Steiner, Y. El-Heri, "The Development of a Reduced-Scale Laboratory for the Study of Solutions for Microgrids", *Energies*, vol. 17, no. 3, 2024, doi:10.3390/en17030609.

[13] E. Hossain, E. Kabalci, R. Bayindir, R. Perez, "Microgrid testbeds around the world: State of art", *Energy Conversion and Management*, vol. 86, pp. 132–153, 2014, doi:https://doi.org/10.1016/j.enconman.2014.05.012.

[14] C. W. Foster, E. A. M. Creeden, S. F. Slocum, F. Yang, "University Microgrid Testbeds: A Literature Survey", *in ICECET*, pp. 1–6, 2022, doi:10.1109/ICECET55527.2022.9872989.

[15] E. Nasr-Azadani, P. Su, W. Zheng, J. Rajda, C. Cañizares, M. Kazerani, E. Veneman, S. Cress, M. Wittemund, M. R. Manjunath, N. Wrathall, M. Carter, "The Canadian Renewable Energy Laboratory: A testbed for microgrids", *IEEE Electrification Mag*, vol. 8, no. 1, pp. 49–60, 2020, doi:10.1109/MELE.2019.2962889.

[16] M. Restrepo, C. A. Cañizares, J. W. Simpson-Porco, P. Su, J. Taruc, "Optimization- and Rule-based Energy Management Systems at the Canadian Renewable Energy Laboratory microgrid facility", *Applied Energy*, vol. 290, p. 116760, 2021, doi:https://doi.org/10.1016/j.apenergy.2021.116760.

[17] M. Z. C. Wanik, "Development of microgrid testbed for real desert environment testing and evaluation: project experience", *IET Conference Proceedings*, pp. 295–301(6), January 2023, doi:10.1049/icp.2023.2751.

[18] M. Mansoor, M. Stadler, H. Auer, M. Zellinger, "Advanced optimal planning for microgrid technologies including hydrogen and mobility at a real microgrid testbed", *International Journal of Hydrogen Energy*, vol. 46, no. 37, pp. 19285–19302, 2021, doi:https://doi.org/10.1016/j.ijhydene.2021.03.110.

[19] T. O. Ajewole, O. E. Olabode, O. S. Babalola, M. O. Omoigui, "Use of experimental test systems in the application of electric microgrid technology across the sub-Saharan Africa: A review", *Scientific African*, vol. 8, p. e00435, 2020, doi:https://doi.org/10.1016/j.sciaf.2020.e00435.

[20] L. Richard, C. Boudinet, S. A. Ranaivoson, J. O. Rabarivao, A. E. Befeno, D. Frey, M.-C. Alvarez-Hérault, B. Raison, N. Saincy, "Development of a DC Microgrid with Decentralized Production and Storage: From the Lab to Field Deployment in Rural Africa", *Energies*, vol. 15, no. 18, 2022, doi:10.3390/en15186727.

[21] A. Alahmed, M. AlMuhaini, "Microgrid Testbed With Hybrid Renewables, Energy Storage, and Controllable Loads", *Arabian Journal for Science and Engineering*, p. 5965–5977, 2023, doi:https://doi.org/10.1007/s13369-022-07152-2.

[22] A. Cagnano, E. De Tuglie, P. Mancarella, "Microgrids: Overview and guidelines for practical implementations and operation", *Applied Energy*, vol. 258, p. 114039, 2020, doi:https://doi.org/10.1016/j.apenergy.2019.114039.

[23] S. Janko, S. Atkinson, N. Johnson, "Design and Fabrication of a Containerized Micro-Grid for Disaster Relief and Off-Grid Applications", *IDETC/CIE*, 08 2016, doi:10.1115/DETC2016-60296.

[24] B. Zhao, X. Zhang, J. Chen, "Integrated Microgrid Laboratory System", *IEEE Trans Power Syst*, vol. 27, no. 4, pp. 2175–2185, 2012, doi:10.1109/TPWRS.2012.2192140.

[25] A. N. Akpolat, Y. Yang, F. Blaabjerg, E. Dursun, A. E. Kuzucuoğlu, "Design Implementation and Operation of an Education Laboratory-Scale Microgrid", *IEEE Access*, vol. 9, pp. 57949–57966, 2021, doi:10.1109/ACCESS.2021.3072899.

[26] M. Kermani, B. Adelmanesh, E. Shirdare, C. A. Sima, D. L. Carnì, L. Martirano, "Intelligent energy management based on SCADA system in a real Microgrid for smart building applications", *Renewable Energy*, vol. 171, pp. 1115–1127, 2021, doi:10.1016/j.renene.2021.03.008.

[27] A. Elhaffar, N. Tarhuni, A. Al-Hinai, "Micro-Grid Educational Laboratory Modernization using IEDs", *in IEEE EDUCON*, pp. 1443–1447, 2022, doi:10.1109/EDUCON52537.2022.9766474.

[28] M. Beus, L. Herenčić, H. Pandžić, I. Rajšl, "Laboratory Setup for Stability and Optimization Studies of Hybrid Microgrids", *in 2022 7th SpliTech*, pp. 1–6, 2022, doi:10.23919/SpliTech55088.2022.9854327.

[29] L. Martirano, M. Kermani, F. Manzo, A. Bayatmakoo, U. Graselli, "Implementation of SCADA Systems for a Real Microgrid Lab Testbed", *in 2019 IEEE Milan PowerTech*, pp. 1–6, 2019, doi:10.1109/PTC.2019.8810795.

[30] J. M. S. Callegari, D. I. Brandao, L. G. Monteiro Oliveira, S. M. Silva, B. J. Cardoso Filho, "Container-Mounted Advanced Microgrid", *in IEEE SPEC/COBEP*, pp. 1–6, 2023, doi:10.1109/SPEC56436.2023.10408010.

[31] T. Caldognetto, S. Buso, P. Tenti, D. I. Brandao, "Power-Based Control of Low-Voltage Microgrids", *IEEE J Emerg Sel Topics Power Electron*, vol. 3, no. 4, pp. 1056–1066, 2015, doi:10.1109/JESTPE.2015.2413361.

[32] J. M. S. Callegari, D. I. Brandao, E. Tedeschi, "Selective PQD Power Control Strategy for Single-Phase Grid-Following Inverters", *IEEE J Emerg Sel Topics Power Electron*, pp. 1–1, 2023, doi:10.1109/JESTPE.2023.3263796.

[33] J. M. S. Callegari, W. F. Souza, D. I. Brandao, T. R. Oliveira, B. J. C. Filho, "The UFMG Microgrid Laboratory: A testbed for advanced microgrids", *Eletrônica de Potência*, vol. 28, pp. 1–11, 2023, doi:10.18618/REP.2023.2.0043.

BIOGRAPHIES

João Marcus Soares Callegari received the doctoral degree in electrical engineering from the Federal University of Minas Gerais, Brazil, in 2024. His current research and technical interests include the design and control of grid-connected multifunctional inverters, the reliability of power electronics-based systems, and AC microgrids. Mr. Callegari was the recipient of the President Bernardes Silver Medal in 2019 and the IEEE IAS CMD Student Thesis Contest 2022 (Non-PhD Category).

Danilo Iglesias Brandao received the doctoral degree in electrical engineering from the State University of Campinas (Unicamp), Brazil, in 2015. He was visiting positions at Colorado School of Mines (2009 and 2013), Università degli Studi di Padova (2014) and Norwegian University of Science and Technology (2018 and 2020). He is currently an assistant professor at Federal University of Minas Gerais (UFMG), Brazil. His main research interests are control of grid-tied converters and microgrids. He is a member of SOBRAEP.

Luís Guilherme Monteiro Oliveira received the degree in Control and Automation Engineering from the Pontifical Catholic University of Minas Gerais - PUC Minas (2002), a Master's degree in Energy, specializing in Photovoltaic Systems, from the University of São Paulo - USP (2005) and a PhD in Electrical Engineering, specializing in Photovoltaic Systems, from the Federal University of Minas Gerais - UFMG (2016). From 2003 to 2005, he worked as a researcher at the Photovoltaic Systems Laboratory (LSF) of the Institute of Energy and Environment (IEE/USP). He also held research positions at the Brazilian Center for the Development of Solar Thermal Energy (GREEN Solar) from March 1998 to December 2002 and from February 2005 to October 2009, as well as at the Solar Materials Laboratory of the Minas Gerais Technological Center Foundation (CETEC) from March to December 2011. Currently, he is Adjunct Professor IV at the Polytechnic Institute (IPUC) of the Pontifical Catholic University of Minas Gerais (PUC Minas) and Professor of the Postgraduate Course (Lato-Sensu) in "Renewable Energy Sources: Generation, Operation and Integration", subject Photovoltaic Systems, and Postdoctoral Resident of the Postgraduate Program in Electrical Engineering (PPGEE) of the UFMG. At this same institution, he also works as a Researcher at the Tesla Laboratory (Power Engineering) and the Energy Conversion and Control Laboratory (LCCE) of the Department of Electrical Engineering of the School of Engineering at UFMG. His expertise lies in the field of Energy, with a focus on Renewable Energy. His main research interests include Photovoltaic Solar Energy (isolated systems, grid-connected systems, distributed generation, and large-scale plants) and Solar Thermal Energy (solar radiation and flat solar collectors).

Sidelmo Magalhães Silva graduated in Electrical Engineering (with a gold medal for the highest GPA), in 1997, and received the Master's and Doctoral degrees from the Federal University of Minas Gerais (UFMG), Brazil, in 1997, 1999, and 2003, respectively, both in Electrical Engineering. From October 2001 to August 2002, he was in the Development Department of ABB Switzerland, Turgi, as a System and Controls Engineer. From August 2017 to July 2018, Prof. Sidelmo was a visiting scholar at the University of Wisconsin-Madison, USA, where he worked with microgrids. Sidelmo M. Silva is a Full Professor at the Department of Electrical Engineering of the Federal University of Minas Gerais. His research interests include power quality, applications of power electronics in electric power systems, microgrids, and renewable energy generation.

Braz J. Cardoso Filho received the Ph.D. degree in electrical engineering from the University of Wisconsin–Madison, Madison, WI, USA, in 1998. Since 1989, he has been a Faculty Member with the Department of Electrical Engineering, Universidade Federal de Minas Gerais, Belo Horizonte, Brazil, where he is currently a Full Professor, and the Founder and the Head of the TESLA Power Engineering Laboratory. He has authored/co-authored more than 300 technical papers on the topics of power electronics and electrical drives and holds 15 patents and patent applications. His research interests include utility applications of power electronics, renewable energy sources, semiconductor power devices, electrical machines and drives, and vehicle electrification.